JOURNAL OF SOLID STATE CHEMISTRY 112, 345–354 (1994)

Synthesis, Characterization, and Acid Exchange of the Layered Perovskites: $A_2Nd_2Ti_3O_{10}$ (A = Na, K)

M. Richard, L. Brohan, and M. Tournoux

Institut des Matériaux de Nantes, Laboratoire de Chimie des Solides, 2, Rue de la Houssinière, 44072 Nantes Cedex 03, France

Received October 29, 1993; accepted December 17, 1993

The structure of the layered perovskite $Na_2Nd_2Ti_3O_{10}$ was investigated by refining X-ray powder diffraction data using the Rietveld method. The Nd^{3+} cation is located in the intraslab perovskite site and the Na^+ cation in the interlayer space. The homologous compound $K_2Nd_2Ti_3O_{10}$ spontaneously intercalates water, and acid exchange of this compound leads to the formation of $H_2Nd_2Ti_3O_{10}$, xH_2O. Prior to condensation at 900°C, the thermolysis of this solid acid yields an intermediate phase which, despite the total removal of water, retains the layered structure from 600 to 850°C. The thermal evolution of the protonated form has been studied by thermal analysis and crystallographic techniques and is found to exhibit two main steps. The first corresponds to the removal of water, which is complete at 600°C, and results in an intermediate phase containing fivefold-coordinated titanium cations and a statistical distribution of Nd^{3+} in the available intra- and interslab sites. The second step can be considered as a complex condensation reaction leading to a 3D-cation defective perovskite.

INTRODUCTION

There is a growing interest in the proton exchange and subsequent dehydration of layered alkali oxides in connection with possible application of the resulting solids in catalysis, photocatalysis, or electrochemistry. For example, this soft chemistry process has been applied to the layered titanates $A'_2Ti_nO_{2n+1}$ (A' = Na, K, Cs; $3 \leq n \leq 6$) to form a metastable form of titania, TiO_2(B), at temperatures below 350°C (1–5).

Two families of lamellar perovskites containing interlayer alkali-metal cations $A'[A_{n-1}B_nO_{3n+1}]$ and $A'_2[A_{n-1}B_nO_{3n+1}]$ have been recently reported. These compounds are related to the Ruddlesden–Popper phases $M^{II}[A_{n-1}B_nO_{3n+1}]$ (6), but exhibit layer charges four and two times weaker, respectively. This lower charge allows ion exchange in an acidic medium and can yield protonated derivatives (7–9). In this paper we report the Rietveld refinement of the $Na_2Nd_2Ti_3O_{10}$ structure, the thermal behavior of $H_2Nd_2Ti_3O_{10}$, xH_2O, and the characterization of the phases that result from its complete dehydration. According to Gopalakrishnan the complete dehydration of $H_2Ln_2Ti_3O_{10}$ leads to a defective perovskite for the lanthanum compound whereas the dehydrated products for Ln = Sm, Gd, and Dy retain their layer-like features before transforming to pyrochlores at 950°C (7). Gondrand and Joubert have also shown that the complete dehydration of $H_2Gd_2Ti_3O_{10}$ leads to a mixture of $Gd_2Ti_2O_7$ pyrochlore and TiO_2 anatase at 900°C (8).

EXPERIMENTAL

The titanates $Na_2Nd_2Ti_3O_{10}$ and $K_2Nd_2Ti_3O_{10}$ were prepared by conventional solid-state methods. Stoichiometric quantities of dried neodymium oxide (preheated at 900°C), TiO_2 (anatase), and an excess (20%) of alkali-metal nitrates ($NaNO_3$, KNO_3) were ground and then pressed to form a pellet which was then fired in Pt crucible in air at 1000°C for 1 day. The products were characterized by X-ray powder diffraction (XRD) using a D5000 Siemens diffractometer in a Bragg-Brentano geometry. Acid-exchange of the potassium parent was achieved at room temperature in an aqueous solution. The powdered titanate was immersed in a 100-fold excess (by weight) of 1 M HNO_3 for 4 days. The resulting product was retrieved by several cycles of centrifugation, washing with distilled water, and finally washing with acetone before drying under vacuum. The thermogravimetric analysis (TGA) experiments were performed under air with a TGS 2 Perkin–Elmer apparatus. The energetics of a structural transformation observed during the dehydration process were measured by differential scanning calorimetry (DSC) using a Perkin–Elmer DSC 4. The experiments were performed under air at a heating rate of 10°/min. The products were analyzed with a TRACOR probe in a 35C Jeol scanning electron microscope. Transmission electron microscopy (TEM) was used to gather electron diffraction data from both acid-exchanged layered titanates and nonhydrated compounds. A CM30 Philips TEM was used to collect diffraction data on specimens prepared by grinding under acetone followed by dispersion onto a holey carbon

0022-4596/94 $6.00

TABLE 1
Experimental Conditions Concerning the XRD Pattern Record of $Na_2Nd_2Ti_3O_{10}$

X-ray wavelengths (Å)	Cu$K\alpha$1, λ = 1,5406
	Cu$K\alpha$2, λ = 1,5444
Sample	20-μm riddled powder
Angular range (°)	11–77
Recording step (°)	0,02909
Recording length	3 hr
Number of calculated reflections	57

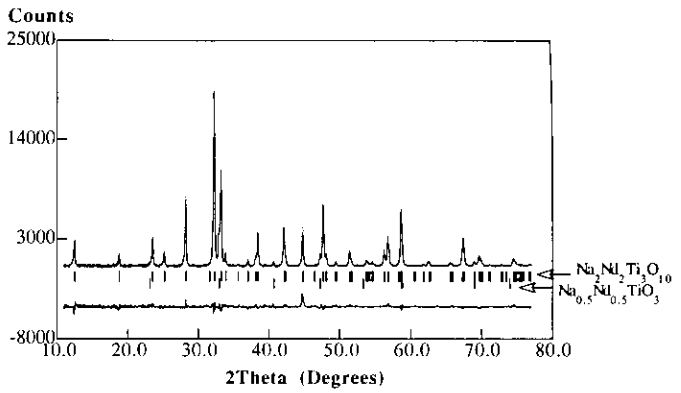

FIG. 1. Experimental, calculated, and difference X-ray powder patterns.

film supported by a copper grid. The relationship between the mother phase and the final product was determined from least-squares refinement of the X-ray powder diffraction data. High-temperature XRD and powder diffraction measurements on samples quenched from high temperature were used to characterize the intermediate structure. AC conductivity measurements of the potassium phase and the new layered titanate $Nd_2Ti_3O_9\square$ were carried with a Solartron 1250 analyzer in the temperature ranges 200–600°C and 100–600°C, respectively. The titanate pellets were previously annealed at 600°C and coated with gold.

$Na_2Nd_2Ti_3O_{10}$: STRUCTURAL DETERMINATION

The X-ray diffraction pattern of $Na_2Nd_2Ti_3O_{10}$ was recorded using a D5000 Siemens diffractometer and the experimental conditions reported in Table 1. The Rietveld refinement of the X-ray powder diffraction data for $Na_2Nd_2Ti_3O_{10}$ was performed in an *I4/mmm* space group beginning with the atomic positions first proposed by Ruddlesden and Popper (6). The Rietveld refinement was conducted using the MPROF program (10). The XRD pattern exhibits some extra peaks which can be attributed to an impurity. These unexplained peaks correspond to the most intense reflections of a cubic perovskite, most likely $Na_{0.5}Nd_{0.5}TiO_3$. This perovskite was included as a second phase in the refinement. After an initial refinement, a difference Fourier map for $Na_2Nd_2Ti_3O_{10}$ was generated from the observed and calculated structure factors. The difference Fourier map was then used to locate Nd^{3+} in the perovskite cavity and Na^+ between the layers. The observed data, final calculated pattern, and profile difference are shown in Fig. 1. Table 2 indicates the refined lattice and atomic parameters.

The interatomic distances within the *I4/mmm* subcell are listed in Table 3 and an idealized picture of the structure is shown in Fig. 3a. The Ti1–O distances show the usual spread of values expected for titanate structures, whereas the Ti2 cation has a relatively long bond to the O2 oxygen (d_{Ti2-O2} = 2.350(1) Å). The weakening of the Ti2–O2 bond may be due to the reinforcement of the Ti2–O4 bond that results from the high basicity of the O4 atom. The sodium atoms occupy an 8 + 1 coordinated site; a short bond is observed with O4, which belongs to

TABLE 2
Final Atomic Parameters from the Rietveld Refinement of $Na_2Nd_2Ti_3O_{10}$

Atoms	*x*	*y*	*z*	*B* (Å^2)	Occupancy
Ti1	0	0	0	−0.08(7)	1
Ti2	0	0	0.1485(1)	−0.08(7)	1
Na	0	0	0.2883(3)	2.4(2)	1
Nd	0	0	0.42531(6)	0.96(4)	1
O1	0	0.5	0	1.0(1)	1
O2	0	0	0.0656(4)	1.0(1)	1
O3	0	0.5	0.1348(3)	1.0(1)	1
O4	0	0	0.2133(5)	1.0(1)	1

Note. a = 3.8182(2) Å; c = 28.369(1) Å; space group, *I4/mmm*; Z = 2; R_{exp} = 0.0706; R_p = 0.166; R_{wp} = 0.1207; R_B = 0.0725.

TABLE 3
Metal–Oxygen Distances in the Structure

M–O	(Å)
Ti1–O1	1.909(1)
Ti1–O2	1.862(1)
Ti2–O2	2.350(1)
Ti2–O3	1.948(2)
Ti2–O4	1.840(1)
Na–O3	2.900(9)
Na–O4	2.7003(3)
Na–O4	2.13(2)
Nd–O1	2.852(1)
Nd–O2	2.712(1)
Nd–O3	2.559(5)

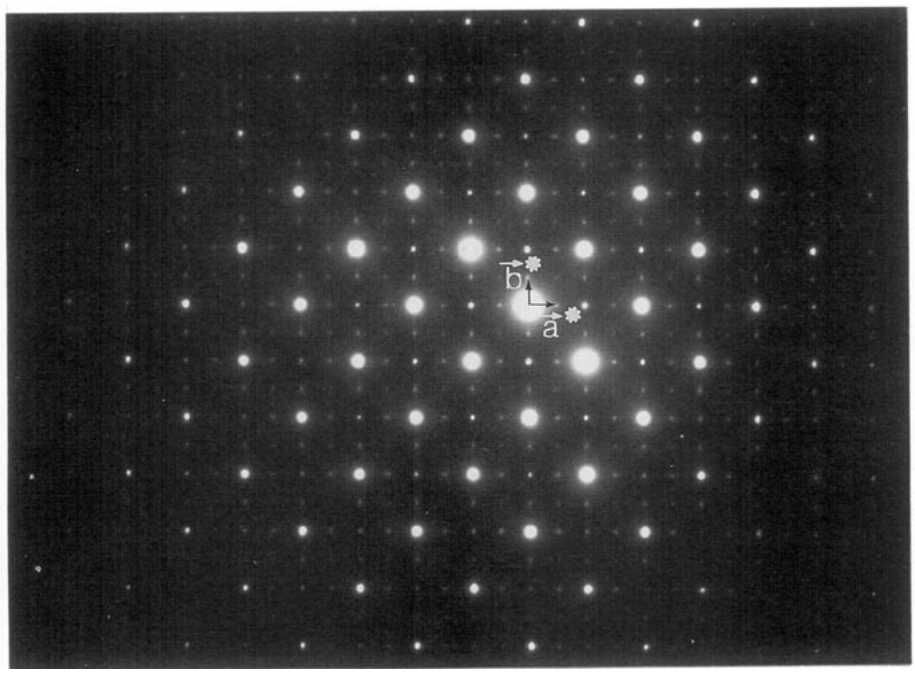

FIG. 2. [001] zone axis electron diffraction pattern exhibiting superlattice reflections along a^* and b^* axes.

the central layer of octahedra of the perovskite slab. The neodymium is 12-fold-coordinated in the intralayer perovskite site where its environment is quite symmetric.

However this description is only that of the average structure and [001] zone axis electron diffraction patterns exhibit superlattice reflections that involve a doubling of the a parameter of the previous tetragonal cell. (Fig. 2) This superstructure is probably due to small atomic displacements resulting from octahedral tilts around b and c axes, which have been frequently reported for many layered perovskites (9) (11). Such a situation is schematically depicted in Fig. 3b. A Rietveld refinement of neutron diffraction data is currently in progress.

$K_2Nd_2Ti_3O_{10}$: WATER INTERCALATION

The two-dimensional structures of the layered titanates allow ion exchange of the interlayer cations and spontaneous water intercalation for $K_2Nd_2Ti_3O_{10}$. The parameters of the anhydrous compound were refined to a = 3.8494(4) Å and c = 29.572(5) Å in an I-centered cell. The increase in the c parameter relative to the Na isomorph is in agreement with the ionic radii difference between the two alkali. The [001] zone axis electron diffraction pattern also exhibits the same extra reflections as the sodium phase and involve a doubling of the a parameter.

The water intercalation capability of $K_2Nd_2Ti_3O_{10}$ was studied at room temperature. Figure 4 shows the number

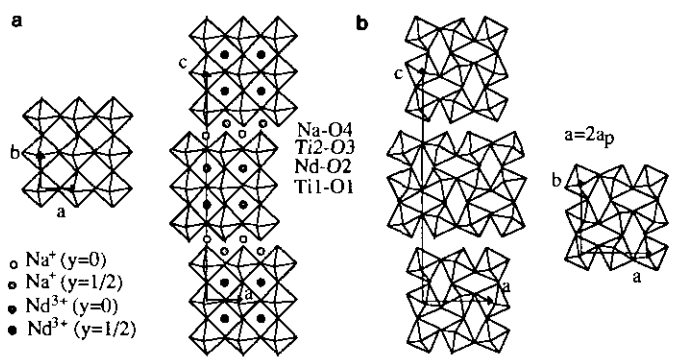

FIG. 3. (a) Atomic notations used for the Rietveld refinement. (b) Schematic representation of octahedral tilts in layered perovskites.

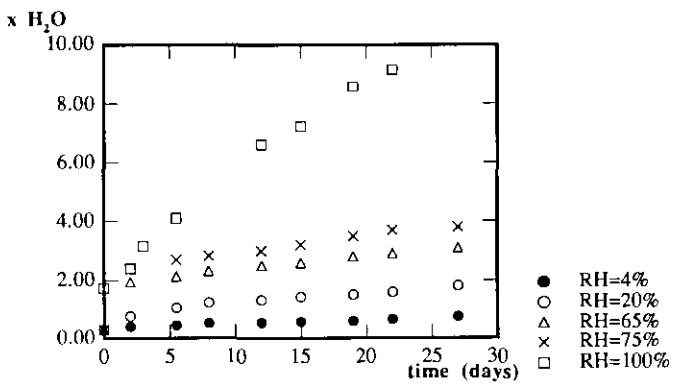

FIG. 4. Number of H_2O molecules per formula unit depending on time for different relative humidity.

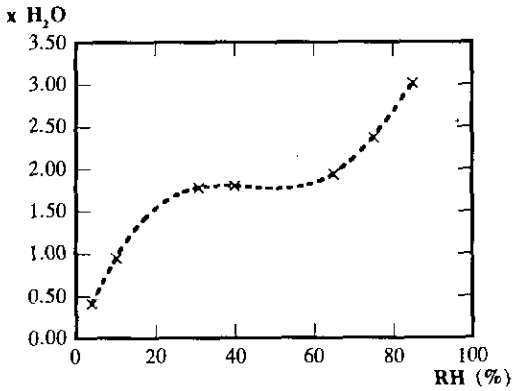

FIG. 5. Number of H_2O molecules per formula unit in various humidity after 2 days.

of H_2O molecules per formula unit x versus time for different relative humidities (RH). No saturation occurs even after 1 month. As shown in Fig. 5, after two days the water content rapidly reaches $x \approx 2$ when RH $\geq$ 30%. The resultant products were characterized using XRD, thermogravimetric analysis, and in some cases transmission electron microscopy. The lattice parameters for different compositions are reported in Table 4. For these hydrated phases the cell becomes primitive due to an $(a + b)/2$ sliding of the central slab relative to the adjacent ones; this was noted previously by Gopalakrishnan (7) for $K_2Nd_2Ti_3O_{10}$, $1H_2O$. Moreover the positions of the

TABLE 4
Evolution of the Cell Parameters for Different x Values in $K_2Nd_2Ti_3O_{10}$, xH_2O Compounds

xH_2O	1 (7)	1.8	3.1	3.8	12
a (Å)	3.843(3)	3.8414(3)	3.8374(4)	3.8369(2)	3.8354(3)
c (Å)	16.68(2)	16.706(3)	16.722(3)	16.715(2)	16.720(2)

extra reflections in the [001] electron diffraction pattern actually imply that an $a_p \sqrt{2}$ parameter should now be used to describe the tetragonal cell (Fig. 6). The angle between the [001] axis in this cell and that of the parent lattice of the tetragonal $I4/mmm$ phase is 45°.

From Table 4 it appears that there is no significant evolution of the c parameter versus x even for $x = 12$. Moreover the TGA trace of this hydrate presents a quasi-plateau corresponding to $K_2Nd_2Ti_3O_{10}$, $2H_2O$ (Fig. 7) which exhibits parameters similar to that of the starting material ($a = 3.8354(4)$ Å and $c = 16.696(2)$ Å). Therefore it appears that an homogeneous intercalated hydrate is formed for $x = 2$ and that the excess water leads to a particle hydrate behavior and an increase in the disorder between the slabs. This hypothesis is supported by the full widths at half height of the (001) reflection lines which broaden from 0.18° to 0.25° when the water content increases. It is possible that this corresponds to a beginning of amorphization due to an increase in the disorder be-

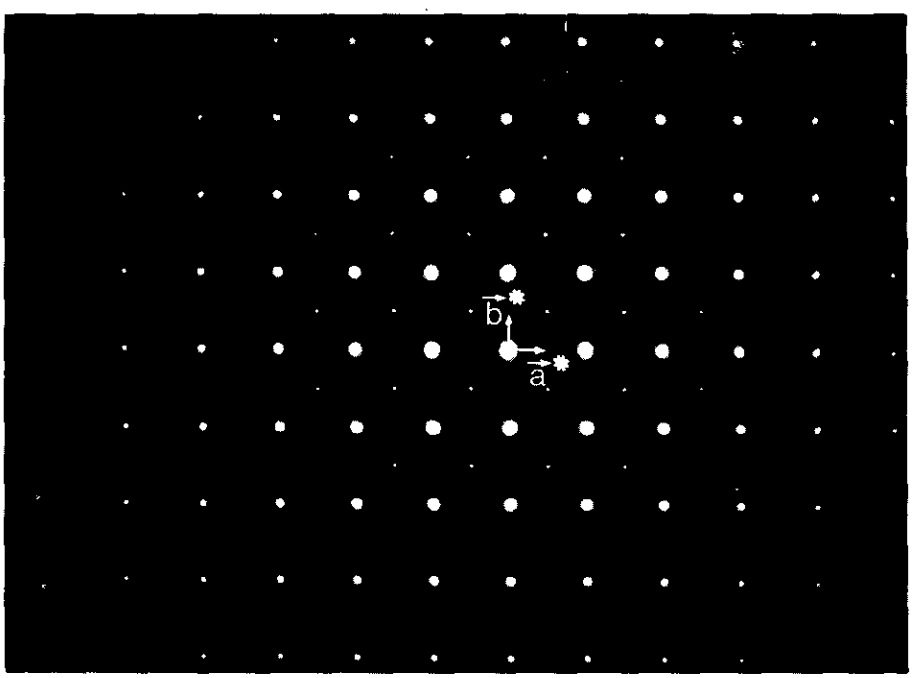

FIG. 6. [001] zone axis electron diffraction pattern for $K_2Nd_2Ti_3O_{10}$, xH_2O.

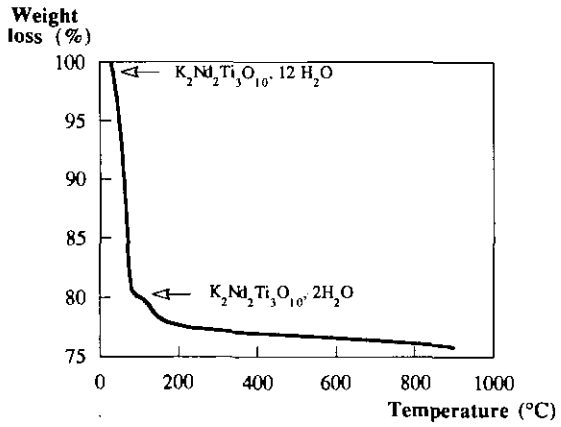

FIG. 7. Thermogravimetric analysis for $K_2Nd_2Ti_3O_{10}$, $12H_2O$.

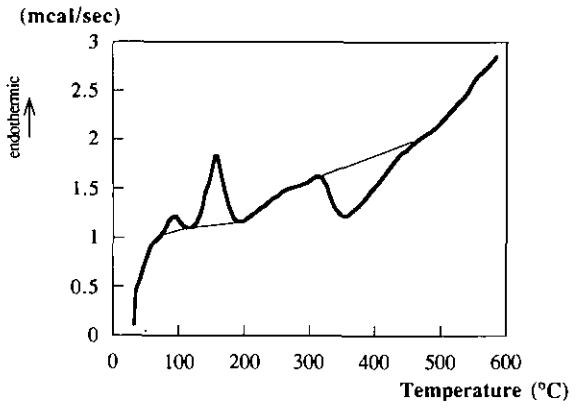

FIG. 8. DSC curve of $K_2Nd_2Ti_3O_{10}$, $3H_2O$.

tween the slabs related to a delamination process. Figure 8 shows the DSC curve of $x = 3$ in the starting material. It exhibits two endothermic peaks that correspond to the water losses, indicating that there are at least two types of water bond in the hydrate. The first peak can be attributed either to adsorbed water or to water present in a disordered intercalated amorphous phase and the second one ($T_{onset} \approx 140$°C) may be due to intercalated water in the $x = 2$ compound. The third exothermic peak is probably due to the gliding of $(a + b)/2$ when the structure reorganizes after dehydration. This latter interpretation is supported by high-temperature XRD measurements. Figure 9 shows that above 400°C the I-centered symmetry of the anhydrous phase is actually restored. Between room temperature and 400°C the X-ray diffraction patterns are rather complicated because of the structural reorganization.

In lower relative humidity (for instance, for RH = 4%) the product corresponding to x values lower than 2 is in fact a mixture of the $x = 2$ hydrate (a = 3.8423(6) Å and

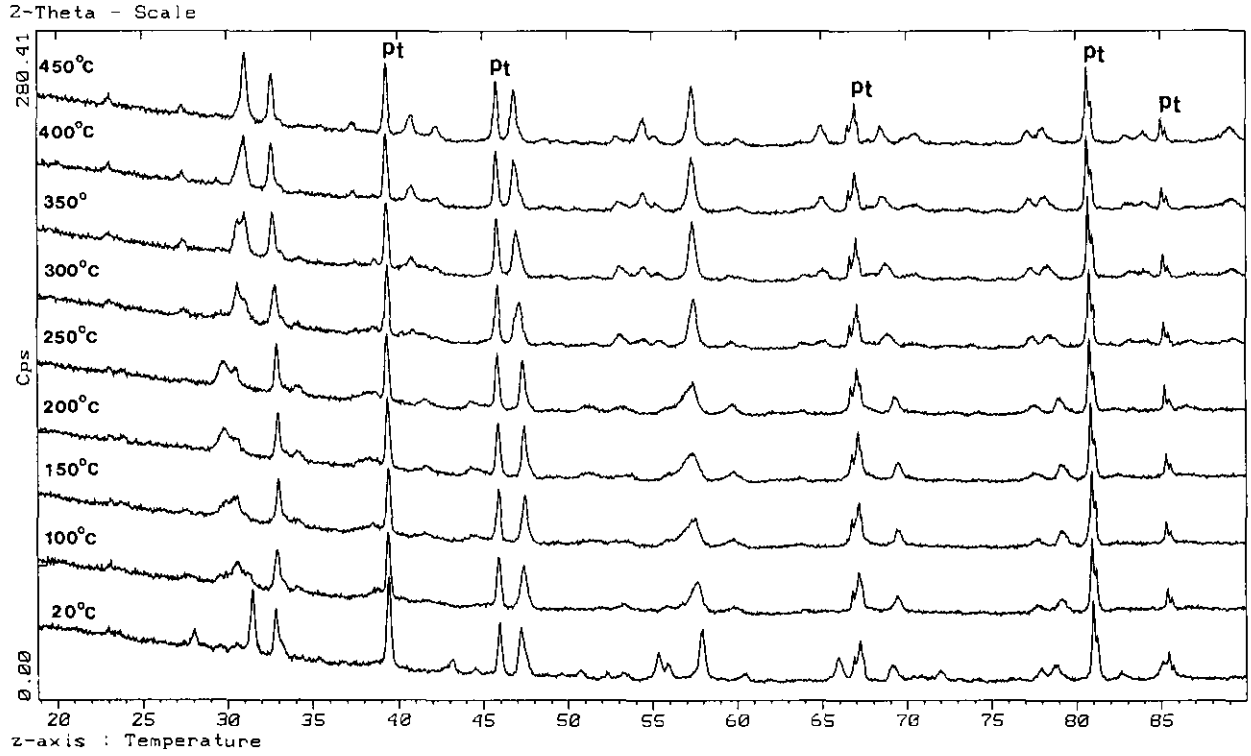

FIG. 9. Thermal evolution of $K_2Nd_2Ti_3O_{10}$, xH_2O X-ray powder diffraction pattern between room temperature and 900°C.

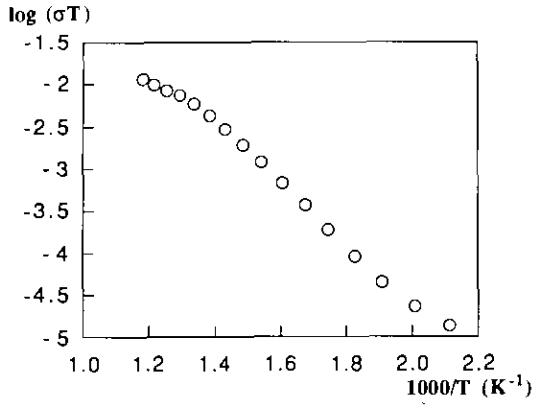

FIG. 10. Conductivity curve for $K_2Nd_2Ti_3O_{10}$.

c = 16.681(5) Å) and the anhydrous parent phase $K_2Nd_2Ti_3O_{10}$.

This anhydrous compound is not a good ionic conductor as shown in Fig. 10. The activation energy (E_a = 0.74 eV) is similar to that of lamellar perovskites $ACa_2Nb_3O_{10}$ (A = K, Cs) exhibiting a lower alkali content (9).

THE PROTONATED PHASE $H_2Nd_2Ti_3O_{10}$, xH_2O

Almost complete exchange of K^+ by protons (more than 98%) in $K_2Nd_2Ti_3O_{10}$ was achieved by stirring the starting layered titanate in excess of 1 M HNO_3 for 2 days. The X-ray powder diffraction pattern, closely related to that of $K_2Nd_2Ti_3O_{10}$, shows the presence of strong (001) lines, indicating that the layered structure is retained (Fig. 11). Indexing the four peaks at d = 13.949, 6.872, 3.752, and 2.675 Å as (002), (004), (110), and (200), respectively, yields a unit cell which is consistent with $a \approx 3.8$ Å and $c \approx 27$ Å. They are estimated by referring to the $K_2Nd_2Ti_3O_{10}$ pattern.

The [010] zone axis electron diffraction pattern shows a $k = 2n + 1$ extinction explained by an $(a + b)/2$ shift of adjacent layers as in $K_2Nd_2Ti_3O_{10}$. The [001] zone axis exhibits some weak extra reflections involving the same doubling of the a_p parameter observed for the anhydrous potassium parent (Fig. 12) and in good agreement with previous data due to Gondrand and Joubert. In addition the enlargement of the 001 reflections observed in electron diffraction experiments can be attributed to a small stacking disorder resulting from the hydroxylation process.

Thermogravimetry for the protonated phase shows multistep weight loss behavior which can be related to the formation of discrete structural intermediates during the dehydration reaction. As shown in Fig. 13, the total weight loss (complete at 600°C) corresponds to 1.7 H_2O leading to the single phase $Nd_2Ti_3O_9\square$. The starting material may be written $H_2Nd_2Ti_3O_{10}$, $0.7H_2O$.

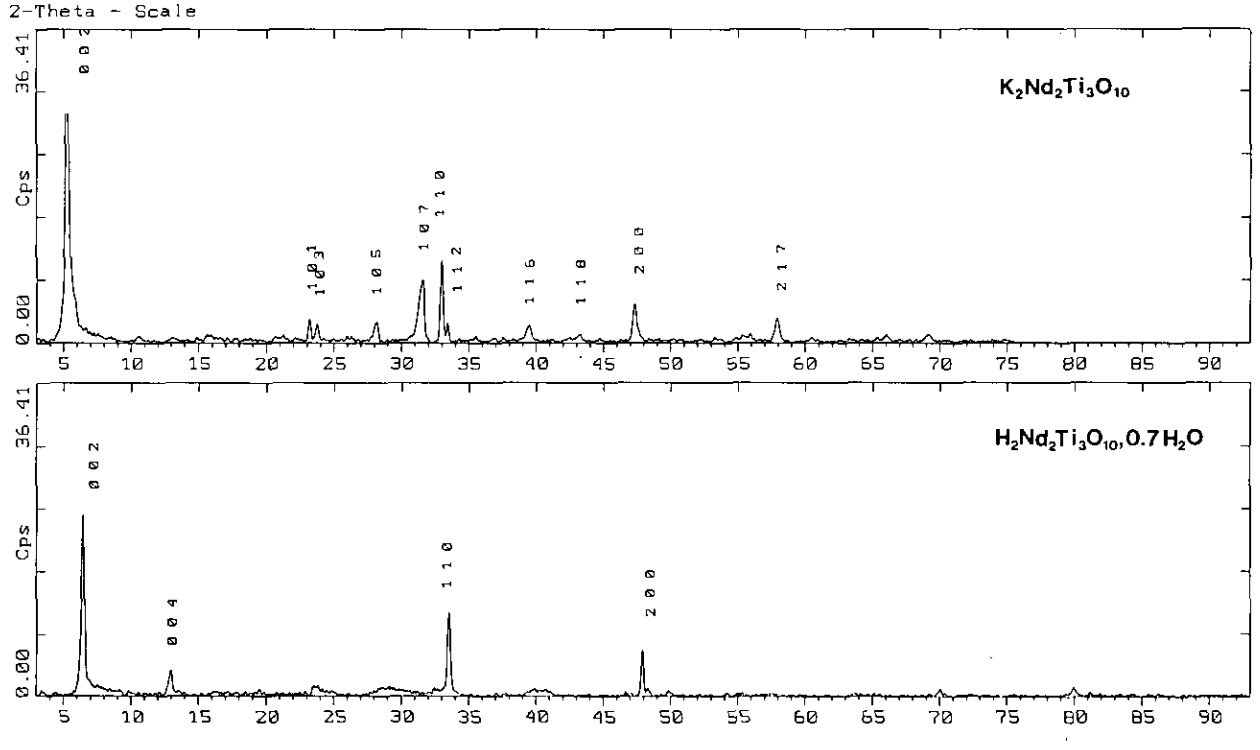

FIG. 11. X-ray powder diffraction patterns of $K_2Nd_2Ti_3O_{10}$ and $H_2Nd_2Ti_3O_{10}$, $0.7H_2O$.

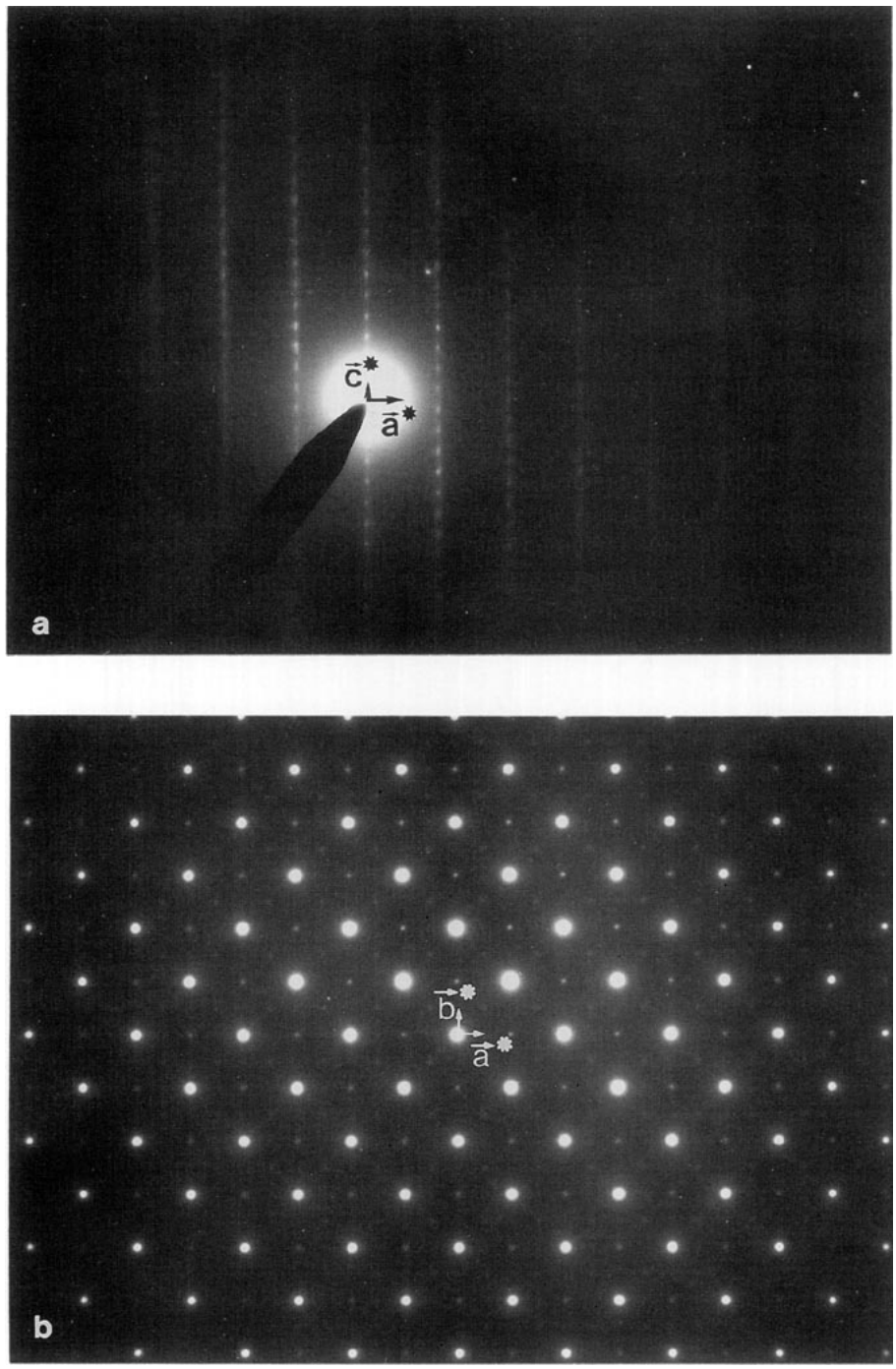

FIG. 12. [010] (a) and [001] (b) zone axis electron diffraction patterns for $H_2Nd_2Ti_3O_{10}$, $0.7H_2O$.

High-temperature *in situ* XRD and powder diffraction measurements on samples quenched from high temperatures were used to isolate and characterize the structures of these intermediates. During the dehydration of $H_2Nd_2Ti_3O_{10}$, $0.7H_2O$ to the 3D-cation defective perovskite $Nd_{2/3}TiO_3$, two distinct structural intermediates were isolated: $H_2Nd_2Ti_3O_{10}$ and $Nd_2Ti_3O_9\square$ at 350°C and 600°C, respectively. Figure 14 shows the diffraction patterns of these intermediates. Between room temperature and 300°C the materials are multiphasic. The refined lattice parameters of the tetragonal *I*-centered unit cell are close to those of the parent layered perovskite in the temperature range 350 to 600°C. The layer-like feature of the structure is thus maintained. However, there is a 10%

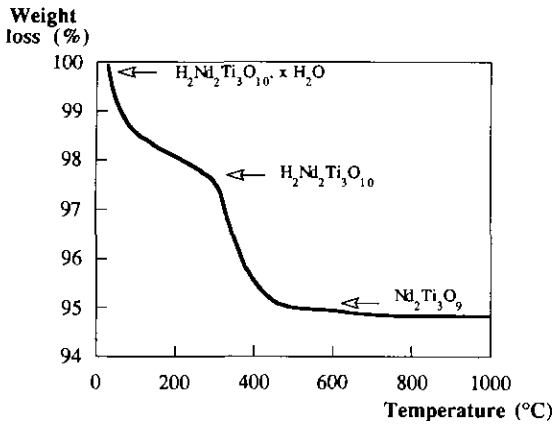

FIG. 13. Thermogravimetric analysis of $H_2Nd_2Ti_3O_{10}, xH_2O$ (x = 0.7).

decrease in the c parameter during the reaction

$$H_2Nd_2Ti_3O_{10},\ 0.7H_2O \rightarrow Nd_2Ti_3O_9\square + 1.7H_2O.$$

The most interesting aspect of this reaction seems to be the conservation of the lamellar structure between 600 and 850°C. In this temperature range, the c parameter decreases by 3% without any significant structural change. The evolution of unit cell parameters and volume from 350 to 850°C is shown in Fig. 15.

TABLE 5
Experimental Conditions Concerning the XRD Pattern Record of $Nd_2Ti_3O_9\square$

X-ray wavelengths (Å)	Cu$K\alpha$1, λ = 1,5406
	Cu$K\alpha$2, λ = 1,5444
Sample	20-μm riddled powder
Angular range (°)	12–95
Recording step (°)	0,02929
Recording length	11 hr
Number of calculated reflections	51

In order to confirm that condensation did not actually occur, a Rietveld refinement of $Nd_2Ti_3O_9\square$ (obtained at 600°C) was performed using the experimental conditions reported in Table 5. Initial refinements using a structure in which the Nd cations were located in the perovskite sites as in $Na_2Nd_2Ti_3O_{10}$ gave an unacceptable reliability factor (R_{wp} = 40.9% for R_{exp} = 7.6%). Therefore several models incorporating different Nd distributions within the perovskite site and in the interlayer space were tested and a structure with 1/3 of the Nd cations in the interlayer space and 2/3 in the layer yielded the best refinement result. In this case the interlayer (0, 0, 0.2363) site is half occupied by the O4 oxygen and one-third by Nd; the final atomic positions are shown in Table 6.

When the neodymium atom is located on the O4 site

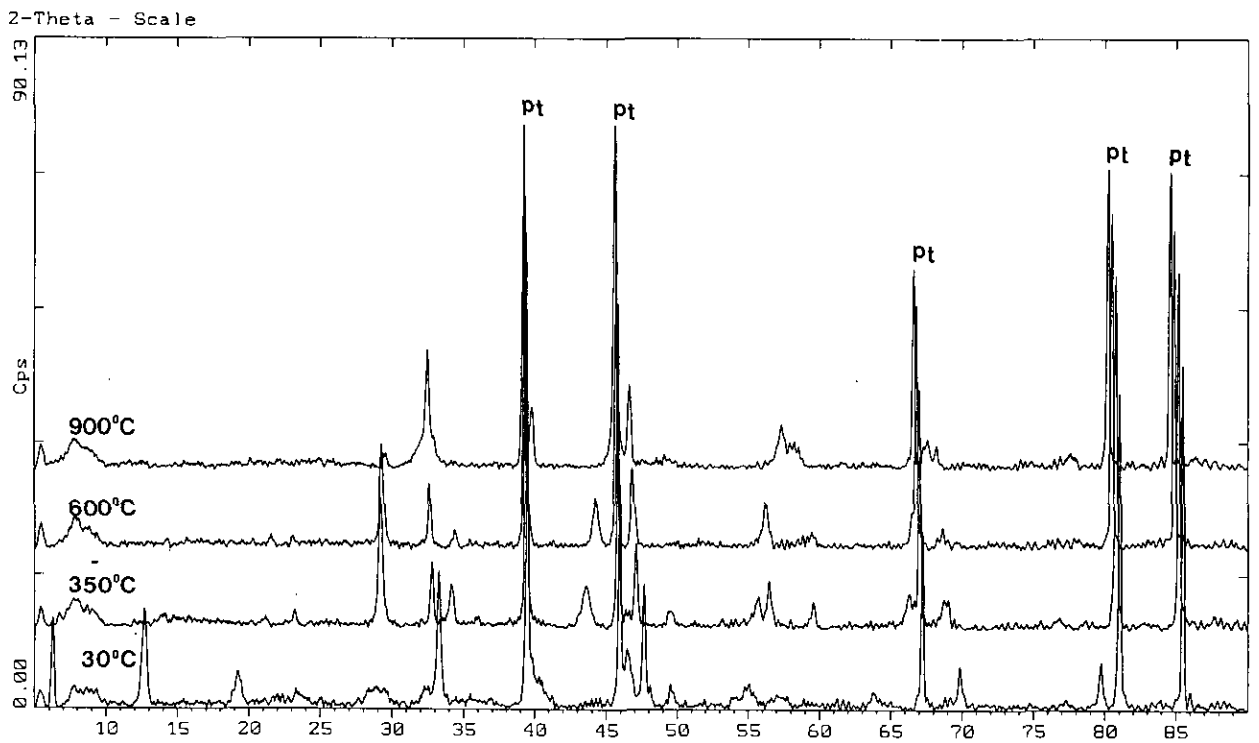

FIG. 14. Thermal evolution of $H_2Nd_2Ti_3O_{10}$, $0.7H_2O$ X-ray powder diffraction pattern between room temperature and 900°C.

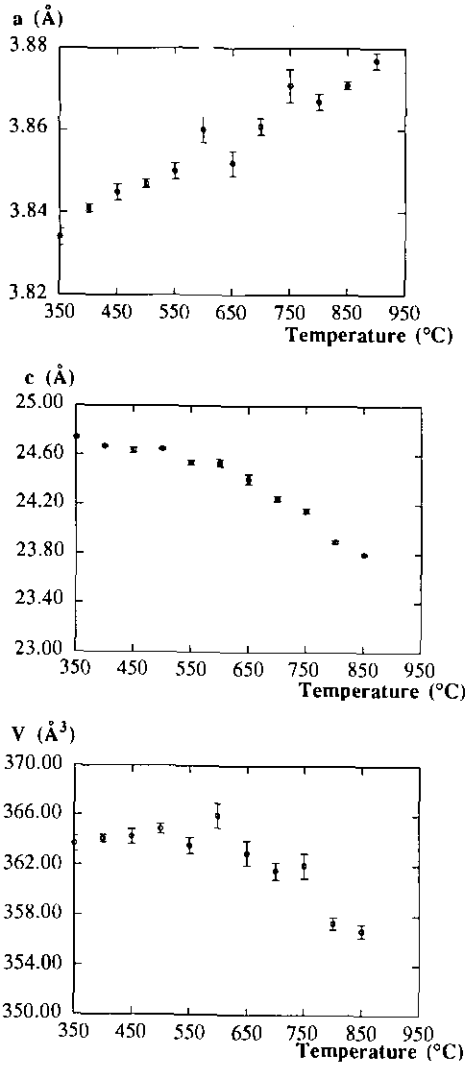

FIG. 15. Evolution of the cell parameters in the 350–850°C temperature range.

the Ti2 titanium atom adopts a fivefold coordination with four O3 neighbors in a square planar arrangement and the fifth oxygen (O2) at the apex of a square pyramid. Fivefold coordination for Ti^{4+} was first found by Anderson and Wadsley in the hygroscopic layered compound $K_2Ti_2O_5$ (12) and has subsequently been identified in Ln_2TiO_5 (Ln = Y, La) (13, 14) and Tl_2TiO_3 (15). This coordination has also been observed in titano-silicates such as $Ba_2TiOSi_2O_7$ (16) or $Na_2TiOSiO_4$ (17, 18). In these compounds the coordination is square pyramidal and in all cases the shortest distance is from the metal to the apical oxygen.

Although this model gave the best fit to the X-ray profile, in order to explain the relatively high values of the reliability factors it must be considered that: (1) considerable disorder between the slabs occurs during the acid-exchange leading to the precursor of $Nd_2Ti_3O_9\square$. This disorder is retained in the dehydrated product as indicated

TABLE 6
Final Atomic Parameters from the Rietveld Refinement of $Nd_2Ti_3O_9\square$

Atoms	x	y	z	B (Å²)	Occupancy
Ti1	0	0	0	3.8(1)	1
Ti2	0	0	0.1558(2)	3.8(1)	1
Nd1	0.5	0.5	0.0915(2)	3.5(1)	2/3
Nd2	0	0	0.2363(3)	2.5(2)	1/3
O1	0	0.5	0	4.2(3)	1
O2	0	0	0.0633(9)	4.2(3)	1
O3	0	0.5	0.163(1)	4.2(3)	1
O4	0	0	0.2363(3)	4.2(3)	1/2

Note. a = 3.8334(6) Å; c = 24.363(4) Å; space group, $I4/mmm$; Z = 2; R_{exp} = 0.076; R_p = 0.291; R_{wp} = 0.195; R_B = 0.1675.

by the widening of the diffraction lines. (2) It is likely that the real symmetry is less than $I4/mmm$; however it is not possible from our experimental data to perform a refinement in a space group with lower symmetry. This point may be a possible explanation for the short value of the Ti2–O2 bond. However despite these potential errors, this refinement allows us to conclude that the condensation of the perovskite layers to give a 3D framework does not occur and that part of the neodymium cations are distributed within the interslab space and the intralayer sites.

The conductivity of $Nd_2Ti_3O_9\square$ is shown in Fig. 16 and is characterized by two different activation energies; the activation energy is almost nil before 300°C and reaches 0.77 eV between 300 and 600°C. At 900°C, the X-ray powder diffraction pattern of the final product can be indexed in a primitive cell with $a = a_p$ and $c \approx a_p$, suggesting cationic disorder inside the perovskite-like cavity.

CONCLUSION

The layered perovskite $Na_2Nd_2Ti_3O_{10}$ exhibits an ordered distribution of the Nd^{3+} and Na^+ cations. The Nd^{3+}

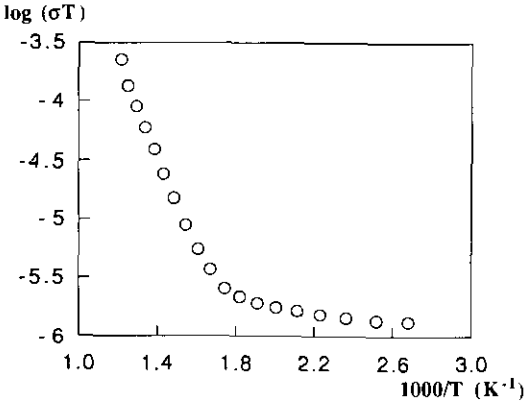

FIG. 16. Conductivity curve for $Nd_2Ti_3O_9\square$.

cations are located in the intraslab perovskite-like cavity whereas the Na^+ cations occupy the site in the interlayer space. The same order exists in the homologous potassium compound, $K_2Nd_2Ti_3O_{10}$. The intercalation of two water molecules leads to an $(a + b)/2$ shift of adjacent layers implying a loss of c doubling and a tetragonal primitive cell. In the protonated form the perovskite layers are linked by hydrogen bonds. The most basic oxygen of the perovskite layer is situated at the periphery of the slab and forms the OH groups in the anhydrous acid form $H_2Nd_2Ti_3O_{10}$; this oxygen (O4), which is bonded to only one titanium (Ti2), is therefore strongly protonated. During the dehydroxylation process between 300 and 650°C oxygen vacancies are formed and one-third of the Nd^{3+} cations migrate from the perovskite site to the interlayer space without any other structural changes, aside from a continuing contraction of c. Finally the condensation of the layers occurs at 900°C leading to a 3D-tetragonal perovskite in which the Nd^{3+} cations are randomly distributed in the perovskite sites.

ACKNOWLEDGMENT

We thank Professor P. Davies for his helpful contribution to the English text.

REFERENCES

1. R. Marchand, L. Brohan, and M. Tournoux, *Mater Res. Bull.* **15,** 201 (1980).
2. M. Tournoux, R. Marchand, and L. Brohan, *Prog. Solid State Chem.* **17,** 33 (1986).
3. T. P. Feist and P. Davies, *J. Solid State Chem.* **101,** 275 (1992).
4. T. P. Feist, S. J. Mockarski, P. K. Davies, A. J. Jacobson, and J. T. Lewandowski, *Solid State Ionics* **28–30,** 1338 (1988).
5. H. Izawa, S. Kikkawa, and H. Koizumi, *J. Phys. Chem. Solids* **86,** 5023 (1982).
6. S. N. Ruddlesden and P. Popper, *Acta Crystallogr.* **11,** 54 (1957).
7. J. Gopalakrishnan, *Inorg. Chem.* **26,** 4301 (1987).
8. M. Gondrand and J. C. Joubert, *Rev. Chim. Min.* **24,** 33 (1987).
9. M. Dion, M. Ganne, and M. Tournoux, *Mater Res. Bull.* **16,** 1429 (1981).
10. A. D. Murray and A. N. Fitch, A Multipattern Rietveld Refinement Program for Neutron X Ray and Synchroton Radiations, 1989.
11. R. Deblieck, J. van Landuyt, and S. Amelinckx, *J. Solid State Chem.* **59,** 379 (1985).
12. S. Anderson and A. D. Wadsley, *Acta. Chem. Scand.* **15,** 663 (1961).
13. M. Guillen and E. F. Bertaut, *C. R. Acad. Sci. Paris B* **262,** 962 (1966).
14. W. G. Mumme and A. D. Wadsley, *Acta Crystallogr. Sect. B* **24,** 1327 (1968).
15. A. Verbaere, M. Dion, and M. Tournoux, *J. Solid State Chem.* **11,** 60 (1974).
16. P. B. Moore and J. Louisnathan, *Science* **156,** 1361 (1967).
17. Yu K. Egorov-Tiamenko, M. A. Simonov, and N. V. Belov, *Sov. Phys. Dokl.* **23,** 289 (1978).
18. P. A. Thomas, *Inst. Phys. Conf. Ser.* **103**(1), 53 (1989).